8 June, 2000
JLAB-TN-00-013

IR FEL Upgrade Driver Accelerator Design, Revision 1.0

D. Douglas

Abstract

The baseline design for the IR FEL Upgrade driver accelerator is documented.

Requirements

A design process for FEL driver accelerators has been discussed elsewhere in some detail [1]. Beam physics requirements for the IR FEL Upgrade driver accelerator have recently been published [2]. Top-level system parameters drawn from this reference are presented in Table 1; an outline summary details accelerator-design-specific requirements.

Table 1: System Parameters

Parameter	*Demo*	*Upgrade*	*Achieved (5/2000)*
energy (MeV)	35-48	80-210	20-48
average current (mA)	5	10	5
charge/bunch (pC)	60	135	135
FEL repetition rate (MHz)	18.75-75	4.6875-75	18.75-75
RMS bunch length (psec)	1/2	1/4	<1/2 (60 pC) ? (135 pC)
peak current (A)	60 A	250 A	>60 A (60 pC) ? (135 pC)
RMS $\delta p/p$ (%)	1/2	1/2	1/4 (60 pC) 1/4 (? 135 pC)
ε_N (mm-mrad)	<13	<30	5-10 (60 pC) ~25 (135 pC)
FEL extraction eff. (%)	1/2	1	>1
Full energy spread after lasing (%)	5	10	>6-8

Summary Accelerator Design Requirements

1) *The accelerator must deliver beam to the wiggler with the phase space appropriately configured so as to drive the FEL interaction*, implying as subsidiary requirements:
   a) dynamically adjustable linear transverse matching into the wiggler,

b) dynamically adjustable linear and quadratic longitudinal matching, *via* orthogonal knobs, into the wiggler, and
c) beam quality preservation during acceleration, transport, and conditioning, such that the Table 1 beam parameters are provided and the following sources of phase space degradation and/or instability are controlled:
   i) lattice aberrations (chromatic/geometric effects),
   ii) accelerator error sensitivities such as
      (1) alignment,
      (2) field quality, or
      (3) excitation errors,
      (4) RF phase errors,
      (5) fundamental power coupler driven head/tail effects, and
      (6) correction of higher order mode coupler driven skew quadrupole coupling,
   iii) coherent synchrotron radiation,
   iv) wakefields, and
   v) space charge.

2) *The accelerator must energy-recover the electron beam after the FEL*, implying as subsidiary requirements:
   a) large transport system acceptance (~10% or more) for "lossless" recovery of the large phase space volume; the system must therefore manage beam transport lattice aberrations (both chromatic and geometric),
   b) dynamically adjustable transverse matching from the wiggler into the linac for energy recovery,
   c) dynamically adjustable linear, quadratic, and cubic longitudinal matching from the wiggler into the linac, *via* orthogonal knobs, for energy recovery and energy compression to order 1% or less at the energy recovery dump,
   d) management of accelerator error sources; the design must conform to an error budget stringent enough to insure that errors such as
      (1) alignment,
      (2) field quality, or
      (3) excitation errors,
      (4) RF phase errors, and
      (5) higher order mode coupler driven skew quadrupole coupling

      do not adversely affect the energy recovery/compression process [3],
   e) management of collective and nonlinear effects, such as
      i) space charge,
      ii) beam break up, and
      iii) the FEL/RF interaction.

3) *Global constraints (some of which are implied by the above requirements) such as the following*:
   a) the upgrade driver should fit within the existing vault and should, insofar as reasonable, allow upgrade activities to proceed in parallel with operation of the IR Demo, thereby maximizing Demo availability and operational lifetime,
   b) the design should exhibit error insensitivity, which in turn suggests
      i) limitation of maximum beam envelopes to ~25 m and that matrix elements and dispersions be limited to manageable magnitudes,

ii) utilization of beam transport system components of adequate acceptance (3" round, at undispersed locations, up to 10" x 3" rectangular at dispersed locations) [4],
iii) use of magnets of modest strength so as to provide gentle bending (radii ~1 m or greater) and focussing (quad focal lengths > ~1 m, limited sextupole field curvatures) so as to avoid untoward chromatic and geometric effects
iv) designing to limit error sensitivities so that IR Demo component specifications are adequate to provide the required system performance,

c) the design should allow good machine operability, using both quantitative modeling and diagnostic-based tuning with orthogonal correction knobs implemented at effective lattice locations,
d) the upgrade should provide global phase advance control/beam envelop control to modify M_{12}, M_{34}, and so forth, so as to maximize BBU thresholds,
e) the recirculation path length should be a 10^{th} subharmonic (plus a half wavelength) of the RF wavelength to support suppression of BBU (*e.g.*, a path length of 630.5 λ_{RF}), and, in contrast (or even in conflict),
f) the recirculation path length should be a half wavelength *near but not at* the 10^{th} subharmonic of the RF wavelength, to support multipass BPM operation (*e.g.*, a path length of 627.5 λ_{RF}).

Machine Concept

The design presented here is for an 80-210 MeV recirculated, energy recovering linac. It is based on available Jefferson Lab SRF technology and comprises a 10 MeV injector, a 70-200 MeV linac based on three cryomodules, and a recirculator providing beam transport and conditioning at a pair of optical cavities and for energy recovery and compression. A layout of the Revision 1.0 machine design (16 May 2000) is shown in Figure 1.

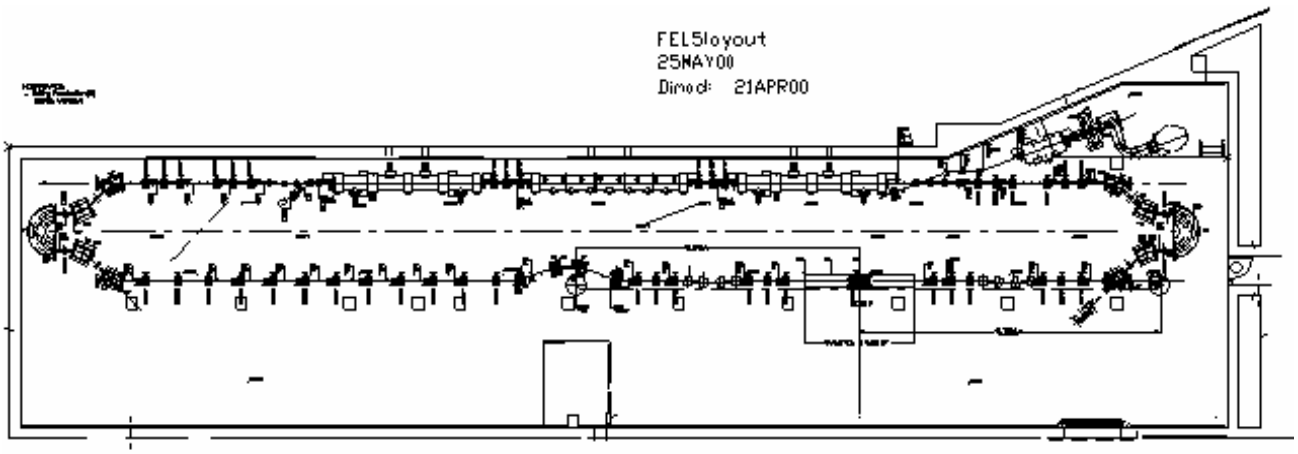

Figure 1: Revision 1.0 machine layout.

The injector consists of a high gradient cryounit using two 5-cell SRF cavities, a betatron matching region, and achromatic, nonisochronous three bend "W" transport line to the

linac. The final dipole of this line serves as well to complete a small reinjection chicane that merges the recirculated (energy recovered) beam path with that of the injected beam. The linac is composed of three cryomodules; the outboard two are traditional 5-cell FEL modules, the middle one uses 7-cell cavities. Beam envelope control is provided by RF focussing of the low energy beams (during both acceleration and energy recovery) and by quad triplets between the modules. A dipole immediately downstream of the third module separates the energy-recovered beam from the full energy beam, directing the former to a dump and initiating a small dogleg in the latter as the start of the recirculator.

After the small extraction chicane, the recirculator consists of transport to the wiggler and energy recovery transport. As CSR did not prove catastrophic in the IR Demo, the FEL insertion is (in the interest of keeping the Upgrade footprint within the vault) in the recirculator backleg. The transport to the wiggler is therefore initially rather similar in structure to the IR Demo recirculator *downstream* of the wiggler. It begins with a region for betatron matching into a Bates-style end-loop; following the endloop a FODO lattice is used to transport the beam to an FEL insertion. This insertion starts at a large dogleg (the "big chicane") around the upstream end of a 32 m optical cavity, and continues with a region for betatron matching into the wiggler. It is followed by another betatron telescope, used to match into an energy-recovery Bates-style endloop. A 16 m optical cavity is embedded in the two betatron matching regions through the use of smaller chicanes (the "little chicanes"). The second end-loop directs the large momentum spread beam following the wiggler to a reinjection matching region, whereafter the aforementioned reinjection chicane merges the energy recovered and injected beams.

Longitudinal matching is accomplished as in the IR Demo. Off-crest (off-trough) acceleration (energy recovery) is used in the linac together with the path length through, and various temporal matrix elements ("momentum compactions") of, the two end-loops to provide the desired beam properties – a short, upright bunch at the wiggler (for high peak current) and a long, small momentum spread "energy compressed" bunch at the dump (to stay within dump acceptance).

A detailed discussion of the design of each of these beam transport modules follows.

Individual Machine Modules

The sequential list of machine beam transport modules utilized in this design is as follows: injector and injection/reinjection line, linac, extraction line/extraction chicane, recirculator (transport to wiggler, energy recovery transport). Each will now be discussed in some detail.

Injector and Injection/Reinjection Line

The 10 MeV injector is based on an upgraded version of present IR Demo electron source and the existing cryounit. This injector is matched to the primary linac using the existing four-quad matching region, to produce at the linac upright phase spaces (with 5 m beam envelopes, as in the IR Demo) in both transverse planes. The beam is transported onto the linac axis using a three bend achromatic but nonisochronous "W" geometry, as in the IR

Demo. The final dipole of this line also completes a chicane that is used to merge the recirculated beam with the injected beam. Unlike the Demo, the Upgrade injection line will use rectangular outboard dipoles. This will allow the use of rectangular dipoles in the reinjection chicane, with an associated increase in the dynamic acceptance of the injected to final energy ratios from the 2:1 – 4.8:1 range in the IR Demo to 8.5:1 – 21:1, which is the requirement for the Upgrade.

The center dipole of the injection line remains a sector bend, as it must focus horizontally for the required dispersion suppression. The bend radius remains 0.6 m and, to retain the existing injector geometry, the bend angle for the injected beam remains 20^o. This highlights two ambiguities in the Upgrade design. First, there will be minor changes in the injection line dispersion due to the use of rectangular outboard dipoles. This can either be tolerated, or it can be completely eliminated by minor changes of the injection line geometry and/or changes in the pole face angles of the center dipole. At present this issue is unresolved; this machine design revision assumes no changes in geometry and thus assumes the remnant dispersion is tolerable. Secondly, the dynamic acceptance of the reinjection chicane is large, but a specific energy must be chosen in order to compute an overall beam path length for the recirculator. We have chosen a nominal energy by noting a 0.6 m bend radius at 10 MeV/c conveniently and memorably translates to a 9.6 m bend radius at 160 MeV/c. The present design therefore assumes an injection momentum of 10 MeV/c and a nominal recirculation momentum of 160 MeV/c. Variations over the full linac working range will induce only minor variations in path length (and focussing), which may be compensated in the recirculator.

The system is shown schematically in Figure 2; preliminary analysis indicates that the use of rectangular dipoles with neither impede betatron matching to the linac nor significantly degrade beam quality via space charge [5].

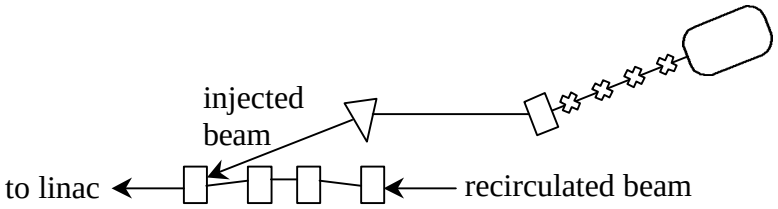

Figure 2: Injector and injection line configuration.

The transverse phase space at the injection point is, as noted, configured by matching across the injection line using the four-quad telescope downstream of the cryounit. The nonisochronous injection line is, in addition, integral to the longitudinal phase space conditioning process. The injector RF components must produce a long, low momentum spread bunch at the front end of the linac in order to induce the bunch-length compression generating momentum/phase correlation imposed on the beam through off-crest acceleration. This is accomplished by an appropriate choice of RF parameters in the injector to produce the desired (essentially upright) phase space at the linac injection

point after transport through the compactional injection line. The dynamics of this process are not at present fully understood, but will be investigated during the remaining IR Demo operating lifetime [6].

Linac

The Upgrade linac consists of three Jefferson Lab cryomodules. The outboard two are 5-cell FEL standard modules – the first is the IR Demo module and the last the FEL module presently installed in the CEBAF south linac. The middle module is a new 7-cell module. Acceleration occurs 10^o off crest (and energy recovery a similar offset from trough) to initiate the required longitudinal matching. Beam envelope control is supplied by RF focussing of the low energy beams in the outboard modules and through the use of quad triplets in the two inter-module warm regions. The optics have been discussed elsewhere [7]; four design features are noteworthy.

1) The useful gradients of the first and final modules are limited by RF focussing of the low energy beams. If the gradients are too high, the beams are over-focussed and the transverse motion is unstable. In the present design, assuming energy gains of 55, 60 and 55 MeV, the phase advance (in either plane) of the accelerated beam through the first module (and the energy recovered beam through the final module) is 0.4 betatron wavelength – near, but not at, the stability limit. Further increases of gradient will lead to betatron unstable motion and result in beam envelope mismatch. This can in principle be compensated by tightly focussing the injected beam, but this solution has potentially unpleasant space-charge consequences. Alternate solutions involve raising the injection and final energy (bad from a system efficiency and radiation-control viewpoint) or more finely segmenting the initial acceleration. One could, for example, use a couple lower gradient cryounits in the linac front and back end so as to "adiabatically" raise the energy and/or introduce compensatory focussing.
2) The present design uses a 5-cell cavity model for the center module, rather than a more precise 7-cell model. This is probably not important at the energies in question (~65 MeV going into the second module) but will become relevant when 7-cell modules become available for the first and final slots; the detailed dynamics become important when accelerating very low energy electrons.
3) The warm region slots and quadrupole layouts of this design revision are configured to support two outboard 5-cell modules and one center 7-cell module. The layout will have to be altered to accommodate future use of 7-cell modules at the linac ends.
4) HOM coupler generated skew quad driven coupling occurs in the 5-cell modules but apparently will not occur in the 7-cell modules. It can be corrected using skew quad trims at each end of the 5-cell modules, but, as the source of the perturbation is RF, this can be done for 1 pass only. The other pass, as it is exactly out of phase with the corrected field, suffers *twice* the skew focussing kick. At present, it is intended to proceed as in the IR Demo and correct the first pass (where beam quality is critical) and allow the coupling to munch the energy-recovered beam. Preliminary simulations suggest that "most" of the coupling of the beam occurs only in the low energy end of the low energy module, so the Upgrade may well not exhibit worse behavior than the Demo in this regard. This observation, coupled with the larger linac energy range of the Upgrade, opens up the possibility of more sophisticated schemes which

compensate one pass in one end of the linac and the second pass in the other. These will be evaluated over the course of the design analysis process.

Extraction Line/Chicane

A dipole chicane is used immediately downstream of the linac to separate the energy-recovered beam from the full energy beam and to direct it to the dump. The geometry is identical to that of the end of the injection line and reinjection chicane. As with the injection line/reinjection chicane, this eases constraints on the ratio of initial to final energy. In analogy with the earlier case, a dumped beam momentum of 10 MeV/c and a full beam momentum of 160 MeV/c is assumed. The dumped beam is bent on a 0.6 m radius orbit through 20^o, the recirculation chicane orbit radius is then 9.6 m. Figure 3 illustrates the scheme.

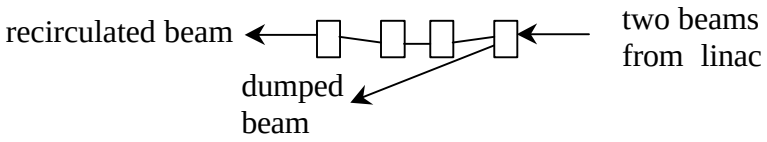

Figure 3: Extraction line geometry.

Recirculator

The recirculator as a whole consists of the transport from the linac to the wiggler and the energy recovery transport. As noted above, a crude analysis of CSR effects suggests that it will be feasible to put the FEL in the machine backleg. This is convenient from various viewpoints, not the least of which is that a three-module linac and 32 m high power optical cavity would not fit in the vault if they were collinear! In addition, placement of the FEL insertion in the recirculator backleg allows use of the recirculation arcs to longitudinally match the beam to both the wiggler (where short bunch length is required) and to the linac, for energy compression and recovery.

We will now discuss the details of the two primary modules; global or integration issues will be summarized after the individual functionality is described.

Transport to Wiggler

The transport to the wiggler starts at the extraction chicane. Following this chicane, a sequence of optics modules is used to transport the beam to the wiggler and condition it to drive the FEL interaction. Sequentially, the optical functions provided by the modules are: matching into the first recirculation arc, recirculation, FODO transport to the FEL insertion, and upstream end of the FEL insertion.

Matching into the recirculation arc – A six quadrupole telescope is used to match transverse beam envelopes to the recirculation arc. Though not absolutely necessary, this match significantly limits beam envelope amplitudes through the recirculation, allows dynamic range for global phase advance adjustment, and thus aids in reducing chromatic aberrations and error sensitivities. The recirculation, discussed in more detail below, is

betatron stable in the vertical plane only; the matching conditions into the recirculator are thus dictated by optimization of global chromatic behavior and, for this lattice revision, are as follows:

1) The horizontal beam envelope should be brought to a waist with amplitude 0.25 m at the symmetry point of the recirculator (at the center of the 180^o dipole).
2) The vertical beam envelopes should be matched to the betatron stable solution for the recirculator.
3) The transverse phase advances should be adjusted to provide optimal chromatic behavior at the wiggler and to render the full machine single turn phase advances either an integer or half integer (to limit BBU effects).

Recirculation Arc – the recirculation arc is a Bates-style endloop. This design was selected because of its success in the IR Demo and the ease of implementing operational tasks such as longitudinal matching. An optimization of bend radii, bend angles, and pole face rotations indicates that in addition to the solution used in the IR Demo (reverse bends with 1 m radius, 30^o angles, and poles at ~¼ of the bend angle), an additional optimum exists with reverse bend radii of 1.2 m, angles of ~45^o, and poles at 0^o and ~1/3 of the bend angle. In this case, the endloop becomes shorter and narrower than in the IR Demo, which is advantageous inasmuch as it leaves space inside the pillars for the high power optical cavity and will allow installation of a significant fraction of the upgrade without interference with Demo operations (see Figure 4 for an overlay of the Demo and Upgrade).

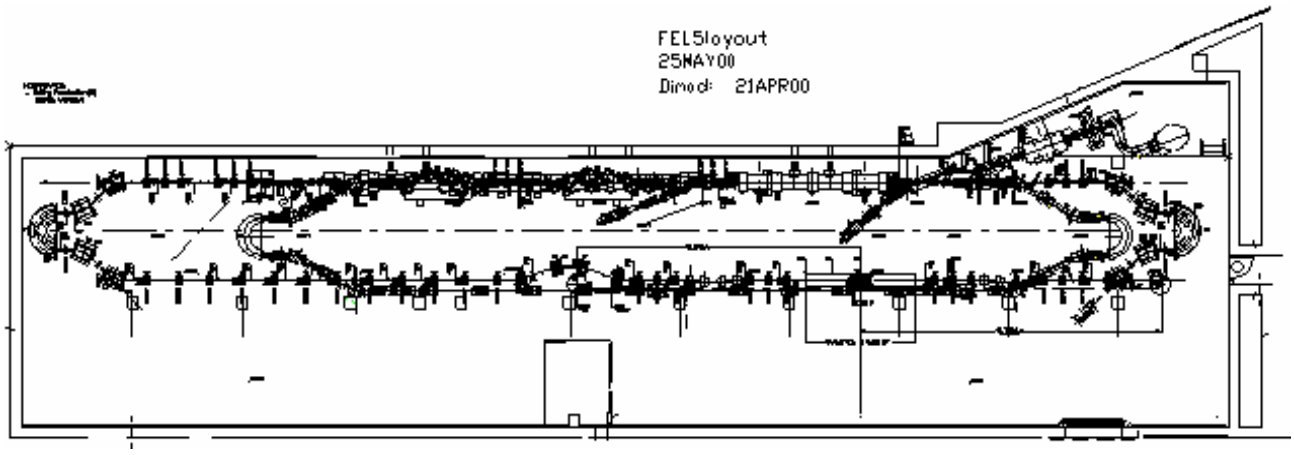

Figure 4: Overlay of Demo and Upgrade in the vault.

As in the Demo, the 180^o dipole has a 1 m radius; the angles, radii and pole faces of the reverse bends were chosen to provide good beam envelopes and chromatic behavior and to conveniently interleave the Upgrade and Demo geometries. The endloop has a native momentum compaction of +0.2 m; when combined with the compaction of the FEL insertion's "big chicane" (about –0.5 m), the resulting negative M_{56} of ~-0.3 m will allow longitudinal matching – bunch length compression – at the wiggler using the same parameter set as was employed in the IR Demo (assuming acceleration of the nominal injected phase space 10^o off crest). The Upgrade endloop will have trim quads and

sextupoles to provide tunable linear and quadratic compactions from linac to wiggler. This feature, unavailable in the Demo, will allow more robust bunch length compression and will, further, allow compensation of RF waveform curvature, with an attendant decrease in bunch length at the wiggler.

FODO Backleg Transport to FEL Insertion – As in the IR Demo, the beam is transported after the first endloop using a FODO quadrupole array. The transport nominally comprises six 90^o FODO cells, but moderate mismatch between the endloop and the FODO lattice has been managed by trimming the front end quads. Such tweaking was also employed to modify the turn-to-turn phase advance and improve chromatic behavior, as well as to limit mismatch at the front end of the FEL insertion. We note here that quite generally, in transport both to and from the wiggler, the phase advance across and amongst the matching telescopes is actively managed to create destructive interferences amongst chromatic aberrations (improving performance at key locations such as the wiggler and reinjection point) and to provide desirable full-turn phase advances. In addition, the quads in the back end of the FODO array were trimmed to manage beam envelopes and reduce betatron mismatch across the big chicane initiating the FEL insertion, with a resultant improvement in error sensitivity and chromatic behavior.

FEL Insertion – The FEL insertion is the interface between the electron beam and the optical cavities, providing both transverse and longitudinal matching at the wiggler. The insertion starts with a big chicane around the upstream end of the optical cavity. This provides clearance between the electron beam and the 32 m high power optical cavity mirrors and momentum compaction to perform the final bunch length compression for high peak current at the wiggler. The size of the chicane is dictated both by the footprint of the optical cavity end can and a desire to generate an M_{56} of –0.5 m. When coupled to the endloop compaction of +0.2 m, this gives a linac-to-wiggler compaction nearly identical to that in the IR Demo (-0.3 m), so that Demo injector performance & acceleration at 10^o off crest will produce the desired short, longitudinally upright bunch at the wiggler.

We note that to this point, the bunch has been fairly long (save for brief periods in the upstream endloop), hopefully alleviating CSR effects. After the big chicane, a six quad telescope (two triplets) matches transverse beam envelopes to the wiggler. The wiggler is assumed to bend vertically and focus horizontally; in this design revision the beam is matched to a waist with 3 m envelopes at the wiggler center. A little chicane between the triplets provides clearance between the electron beam and the upstream mirror of a 16 m broadband optical cavity.

The FEL insertion is completed by a downstream matching telescope, which is properly part of the energy recovery transport.

Energy Recovery Transport

Immediately following the wiggler, the electron beam retains a very short bunch length but has a very large momentum spread (as high as 10%). This must be cleanly transported for energy recovery; the energy recovery itself must generate an energy compression to

prevent adiabatic antidamping from generating an unwieldy momentum spread at the dump. The energy recovery transport is thus most clearly defined by the large momentum acceptance required of it and by its need to properly configure the longitudinal phase space for energy recovery and energy compression. This process requires the transport provide independently tunable momentum compactions through third order so as to compensate both lattice and RF waveform variations in path length/time of flight/RF phase with momentum. Sequentially, the operations in the energy recovery transport are: matching to the energy recovery recirculation (which is also the final operation in the FEL insertion), the recirculation arc, and a reinjection matching. Large energy acceptance is provided by the use of a Bates-style endloop, identical to that in the linac-to-wiggler transport, coupled with judicious choice of phase advances through the matching telescopes. As in the linac-to-wiggler transport, this creates destructive interferences amongst beam envelope chromatic aberrations, improving overall performance.

Match to energy recovery recirculation arc/completion of FEL insertion – Following the wiggler, a six-quad telescope (two triplets) matches the transverse beam envelopes from the wiggler to the energy recovery recirculation arc. The matching conditions are specified as in the linac-to-wiggler transport, and will be reviewed in the next section. At this point, the electron bunch is still short, but has a very large momentum spread (of up to 10%). The phase advances in this telescope (as in those of the transport to the wiggler) are adjusted to help create destructive inteferences of chromatic aberrations through the wiggler-to-linac transport and thereby to improve chromatic performance. The optical mode in the 32 m optical cavity and the electron beam are coaxial through this telescope; a little chicane between the triplets provides clearance between the electron beam and the downstream mirror of the 16 m optical cavity. As this telescope is common to the optical cavity axis, it is properly considered the concluding portion of the FEL insertion as well as the first module of the energy recovery transport.

Energy-recovery recirculation arc – Recirculation for energy recovery is accomplished through the use of a Bates-style end loop identical in layout to that employed in the linac-to-wiggler transport. As noted in the previous discussion, endloop parameters were established though an optimization process designed to achieve the requisite momentum acceptance. In addition, the Bates geometry provides large momentum acceptance, through the use of trim quads, sextupoles, and octupoles, independently tunable linear, quadratic, and cubic momentum compactions (M_{56}, T_{566}, and W_{5666}). The match into this arc is specified by the same conditions as in the upstream end – namely, an upright horizontal phase ellipse with horizontal envelope amplitude of 0.25 m, matching to the betatron-stable vertical matched beam envelopes, and overall phase advance selected to provide adequate chromatic behavior by generating cancellations amongst chromatic aberrations. The first dipole of the endloop bends the electron beam off the axis of the optical mode, providing the separation required for the introduction of the downstream end can of the 32 m optical cavity.

The longitudinal match is supported by the nominal endloop M_{56} of +0.2 m; this is the same value as used in the IR Demo and is known to provide (with off-trough energy recovery) good energy compression at the end of the linac. Run-time tunable

compensation of RF waveform slope, curvature, and torsion is provided by the aforementioned trim elements. As noted above, longitudinal matching will proceed in the Upgrade just as in the Demo; a review of this process is given below.

Global/Integration Issues

A plot of beam path positions is shown in Figure 5. Figure 1 illustrates the driver, with conceptual major beamline components, in the vault. The recirculation path length of this Revision 1.0 design is 630.5 λ_{RF}; as noted in requirement 3)e and 3)f, this is probably desirable from an instability (BBU) viewpoints but not optimal for multipass BPM operation.

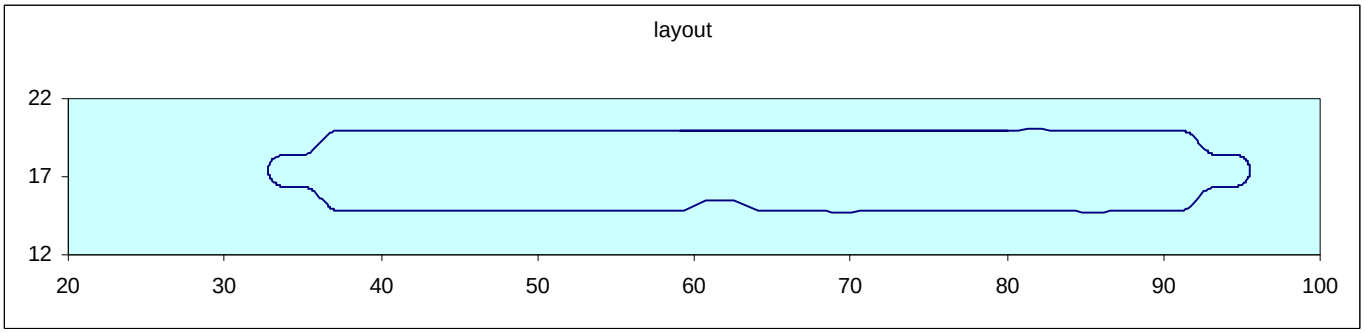

Figure 5: Beam path positions.

This design revision reflects an attempt to leave adequate beamline space for diagnostics, correctors, and trim elements. A forthcoming JLAB-TN will discuss diagnostic and correction systems. System specifications are detailed in a reference DIMAD output file, available through links at http://www.jlab.org/~douglas/FELupgrade/masterindex.html. Worthy of note is the maximum quadrupole strength; in TRANSPORT notation, $k_1^{max}<7/m^2$, so that at 210 MeV/c, the maximum required gradient is 49 kg/m or 490 g/cm. This is apparently within the range of a preliminary design for the 3"x 15 cm quad driven by a 10 A power supply [8].

As noted in previous sections, though the design is functionally modular (in that it supports localized matching regions into and out of the endloops and wiggler), global suppression of aberrations and thresholds is accomplished through adjustment of phase advances between various points of the machine. All telescopes use six quads to provide degrees of freedom beyond the four required for simple beam envelope matching (β_x, α_x, β_y, α_y). This allows adjustment of betatron phase through the telescopes, across the endloops, and turn-to-turn. An appropriate choice for evolution in phase advance (chosen through simulation-based optimization – *i.e.* tweaking and twiddling) results in destructive interference of chromatic aberrations in beam envelopes and providing integer (or half integer) phase advances from turn to turn in the linac, with (hopefully) an associated improvement in BBU thresholds.

Longitudinal matching is supported using the IR Demo parameter set [9]. Acceleration in the linac is performed 10^o off crest. The linac-to-wiggler transport M_{56} of –0.3 m then acts in concert with the resulting phase-energy correlation to rotate the longitudinal phase space, producing a short, upright bunch at the wiggler. The process is illustrated schematically in Figure 6. We note that the Upgrade will require a shorter bunch at the wiggler than that used in the IR Demo. Consideration of Figure 6 indicates that the bunch length at the wiggler is proportional to the momentum spread at the injector, while the momentum spread at the wiggler is proportional to the bunch length at the injector. It is therefore likely that in the Upgrade the injector will run with halved momentum spread and doubled bunch length. This will aggravate longitudinal aberrations such as RF waveform curvature and $T5_{66}$; it is anticipated that these must be compensated through use of trim quads and sextupoles in the linac-to wiggler transport [10]. Following the wiggler, the phase space is slewed for energy recovery and compression using the recirculator native compaction of +0.2 m. The large induced momentum spread in the Upgrade (10%) will likely require the use of at least one family of octupoles for the correction of RF waveform and beam transport lattice induced longitudinal torsion. This is illustrated both in Reference [9] and in simulations discussed below.

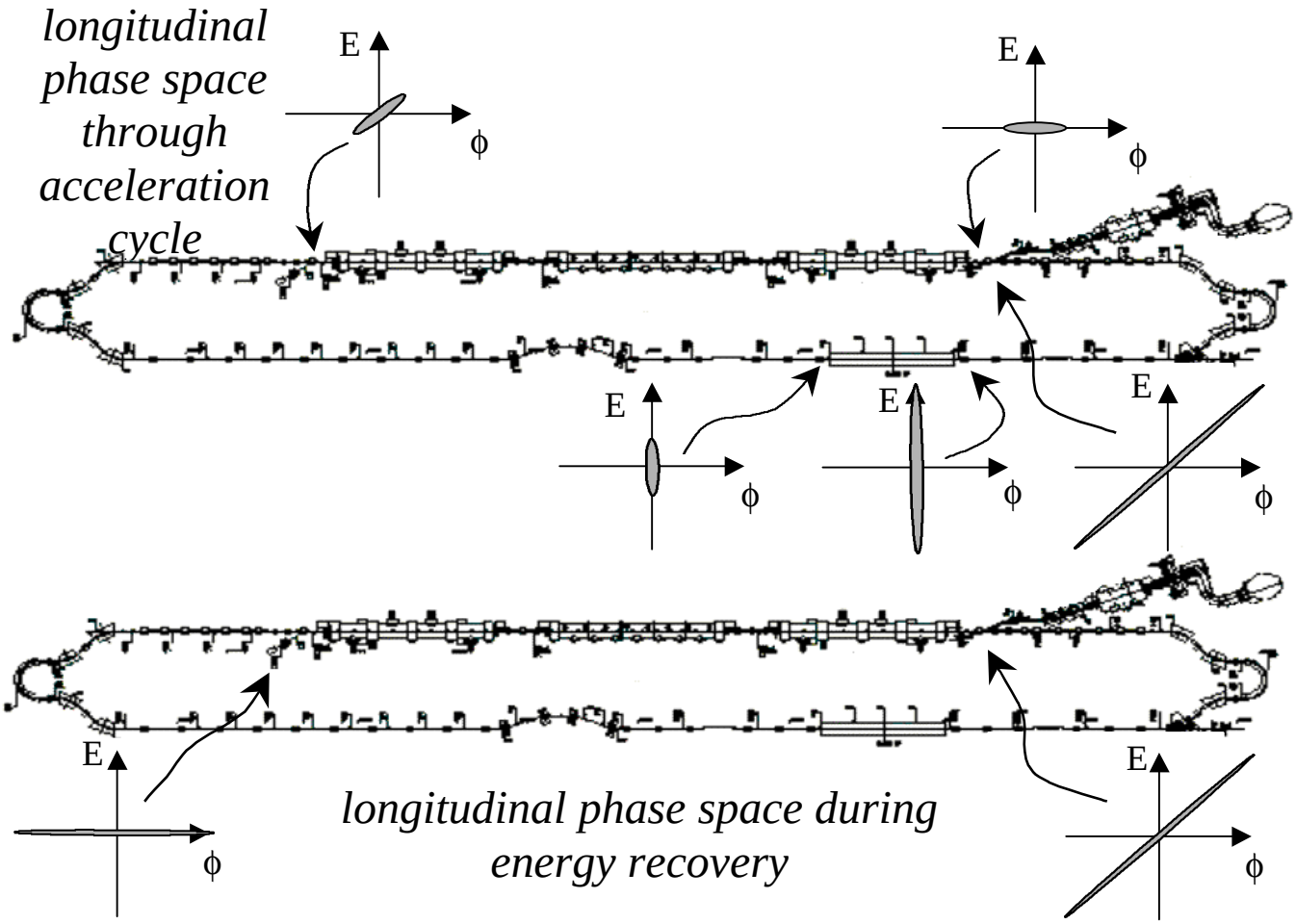

Figure 6: Longitudinal matching scenario in the Upgrade.

Performance

System performance is undergoing analysis; preliminary results suggest all requirements will be met. Figure 7 shows beam envelopes through the system, from injector to extraction point. Design injection conditions ($\beta_{x=}\beta_y$=5 m, $\alpha_x=\alpha_y$=0) are assumed. Figure 8 gives the rms beam spot sizes from linac back to linac for this lattice solution, assuming the maximum allowable normalized emittance of 30 mm-mrad, an rms momentum spread of ½% up to the wiggler center and an rms momentum spread of 2% beyond the wiggler center, and longitudinal phase space matched to provide the desired ½ psec FWHM (60 μm rms) bunch length at the wiggler.

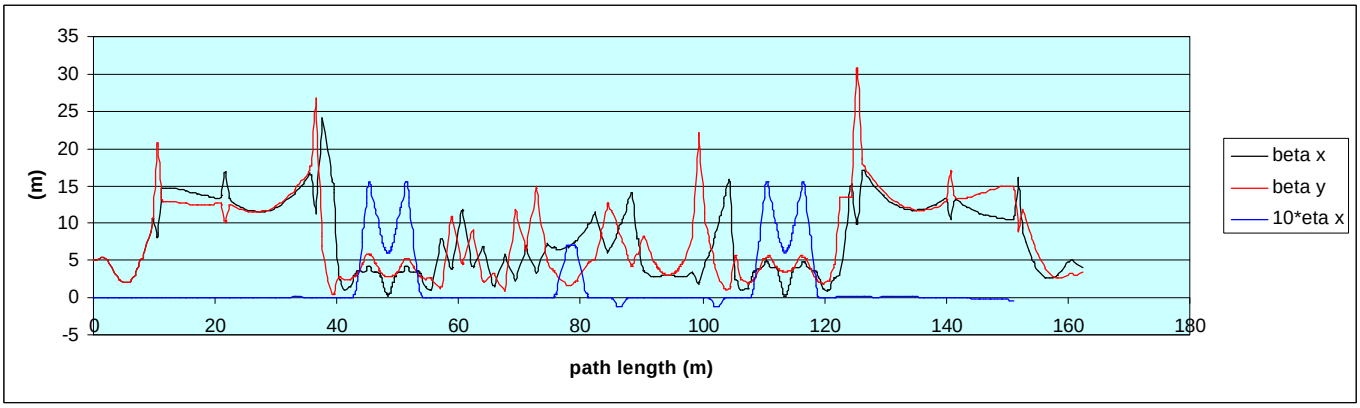

Figure 7: Beam envelope functions, injection point to extraction point

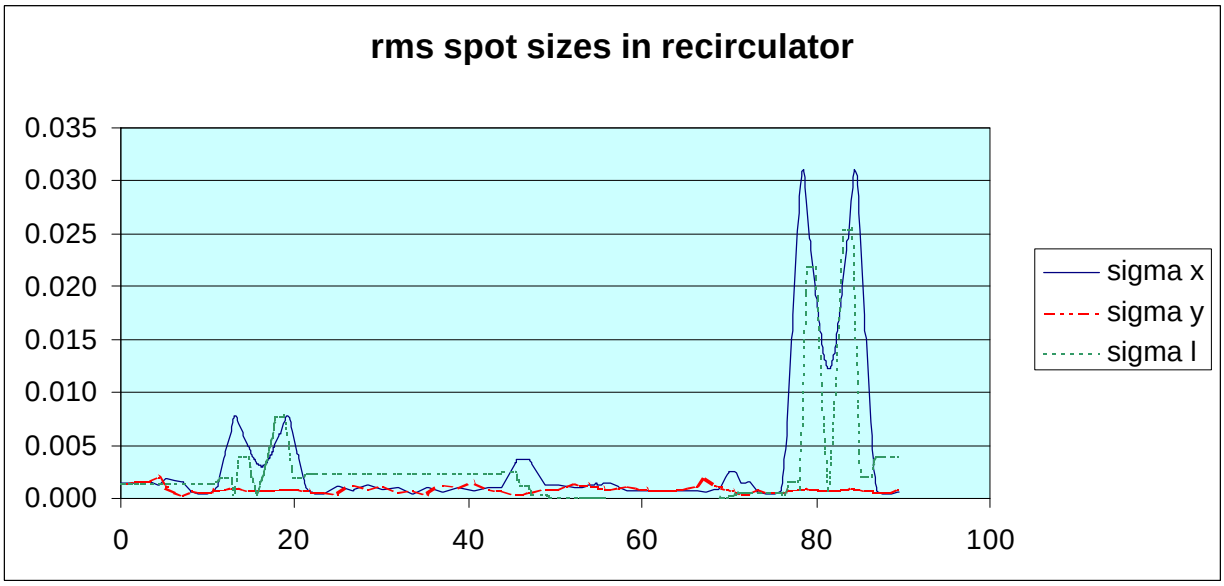

Figure 8: RMS spot sizes, linac to linac, for emittance of 30 mm-mrad and

An aberration analysis characterizing both chromatic and geometric behavior from linac to wiggler and wiggler to linac has been performed. Figure 9 gives the results of a momentum scan of the linac to wiggler transport over a ±1.5% momentum bite; Figure 10 shows the results of a geometric aberration analysis for the same momentum interval at 10 times the nominal maximum normalized emittance of 30 mm-mrad (and an energy of ~100 MeV). Both variations are, at this preliminary stage of design and analysis, acceptable. Figure 11 shows both the horizontal central orbit variation at the wiggler over the indicated momentum interval and the path length variation. As the orbit variation is small and the path length variation linear, both are, at the present, acceptable as well.

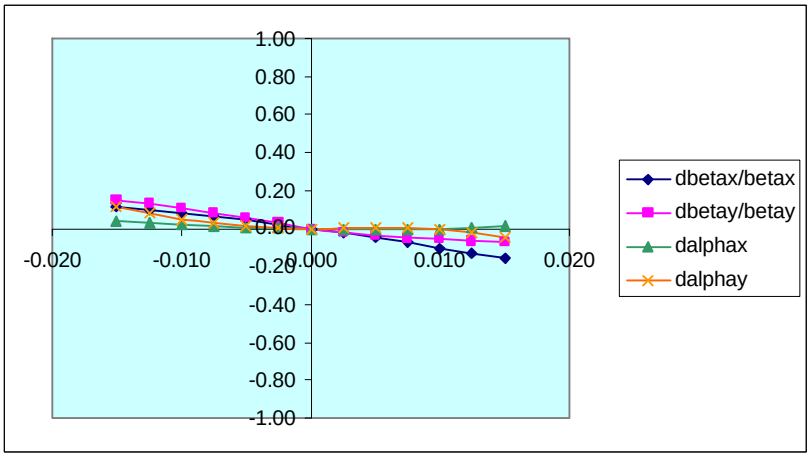

Figure 9: Momentum scan – linac to wiggler transport.

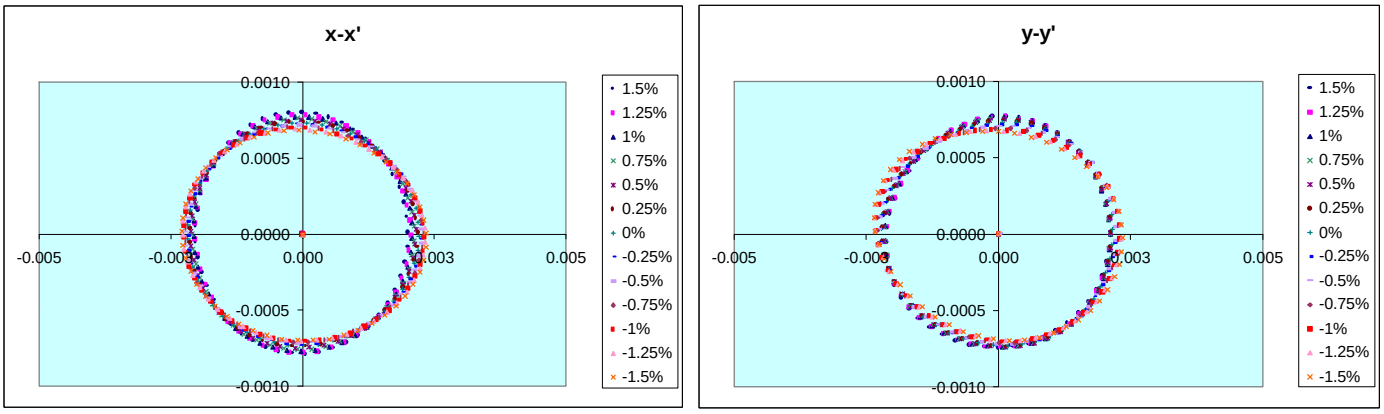

Figure 10: Geometric aberration analysis; 10 x 30 mm-mrad normalized emittance (at 100 MeV) over momentum interval of Figure 9 in ¼% bites.

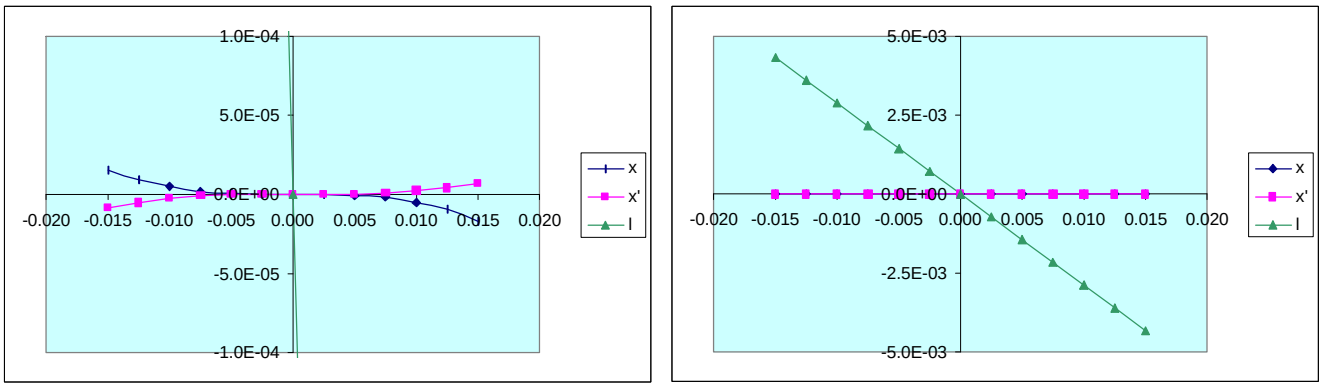

Figure 11: Central orbit variations at wiggler over Figure 9 momentum interval. Left figure: variation in horizontal position and angle; right figure: path length variation.

Results of an analogous analysis for the wiggler to reinjection transport are presented in Figures 12 through 14. Figure 12 gives momentum scan over a ±6% momentum bite; Figure 13 shows the results of a geometric aberration analysis for the same momentum interval at 10 times the nominal maximum normalized emittance of 30 mm-mrad (and an energy of ~100 MeV). Both variations are, at this preliminary stage of design and analysis, rather large but probably acceptable. Figure 14 shows the horizontal orbit variation at the wiggler over the indicated momentum interval and the path length variation. The orbit variation is modest and acceptable but the path length variation shows some deviation from linearity, consequences of which will be illustrated by tracking results to be given below.

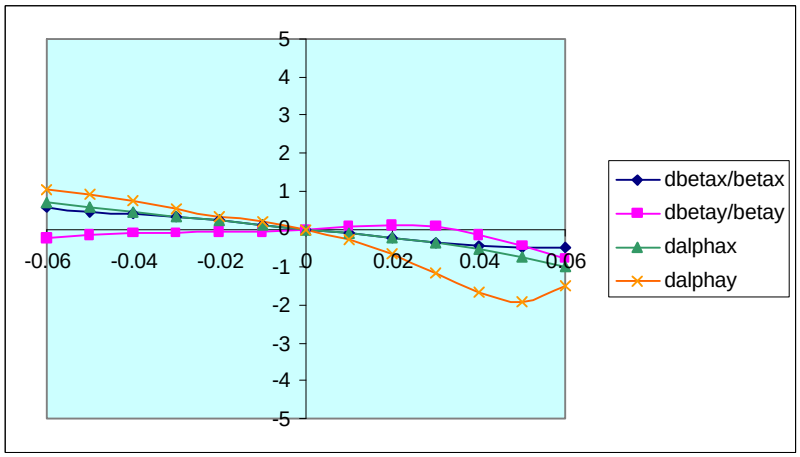

Figure 12: Momentum scan for wiggler to reinjection transport.

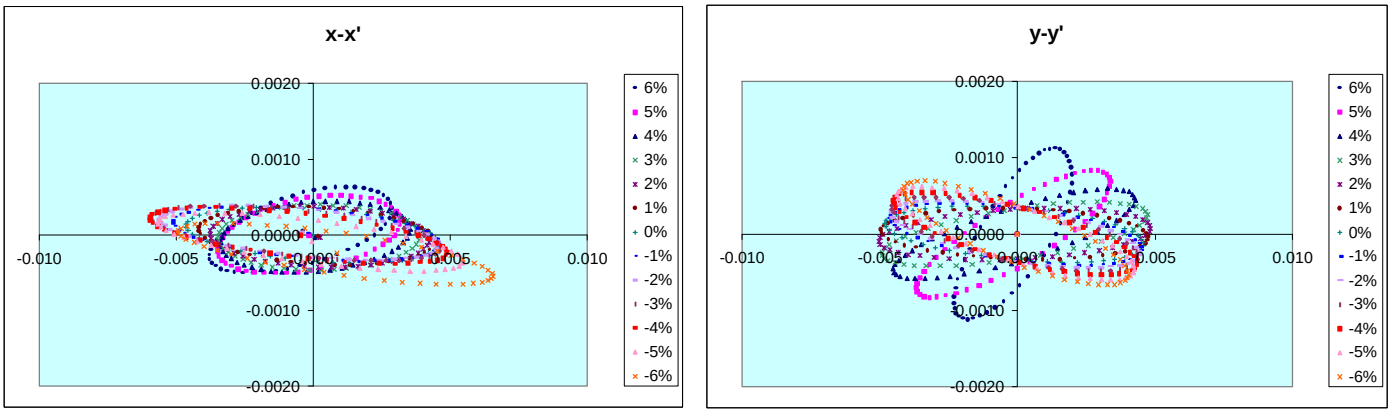

Figure 13: Geometric aberration analysis; 10 x 30 mm-mrad normalized emittance (at 100 MeV) over momentum interval of Figure 12 in 1% bites.

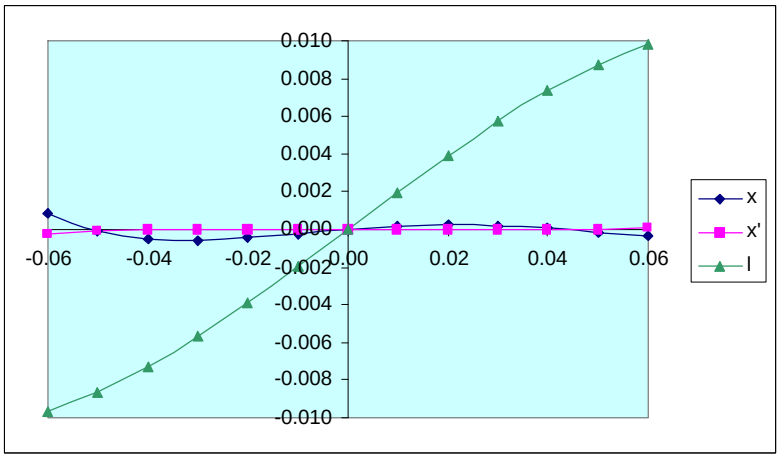

Figure 14: Central orbit variations at wiggler over Figure 12 momentum interval. Note torsional deviation of path length from linearity.

A ray tracing check of the energy recovery process was performed. Figure 15 presents results of this simulation for the Revision 1.0 optics solution. Initial conditions assume upright transverse beam ellipses at the wiggler center, with beam envelope amplitude of 3 m, a longitudinally upright phase space with 60 μm rms (0.2 psec) bunch length and 2% rms momentum spread. An rms normalized emittance of 30 mm-mrad was used and a six sigma Gaussian distribution of 500 particles generated and traced to the extraction point, with outputs at module ends and middles.

We find that the beam is well confined transversely through the energy recovery process until the end of the linac, where, due to adiabatic antidamping, the large emittance becomes apparent. This encourages the use of 3" vacuum chamber; footprints of 2" and 3" chambers are superposed on the final transverse profile plot in Figure 15g. Longitudinally, the path length illustrated in Figure 14 manifests itself in the evolving

momentum tails, leading to a very large full momentum spread at the dump. These tails are readily suppressed through use of a single octupole family to compensate the lattice W_{5666}; results with this compensation are shown in Figure 16, and indicate that octupoles will be both necessary and effective. We note that in this DIMAD simulation this phenomenon is solely due to the lattice; in the actual machine RF waveform torsion will be significant and will require compensation as well [11].

Preliminary results including HOM coupler generated skew quad driven coupling in the 5-cell modules suggest local compensation will effectively preserve beam quality during acceleration and will not fatally degrade beam quality during energy recovery. Figure 17 shows the results at the end of energy recovery cycle with skew quads and first pass compensation activated. (We remark that these results are for a preliminary lattice version for which the linac optics are the same as in the Revision 1.0 solution.) A more detailed study quantitatively characterizing this effect will be performed as a part of the ongoing Upgrade design effort [12].

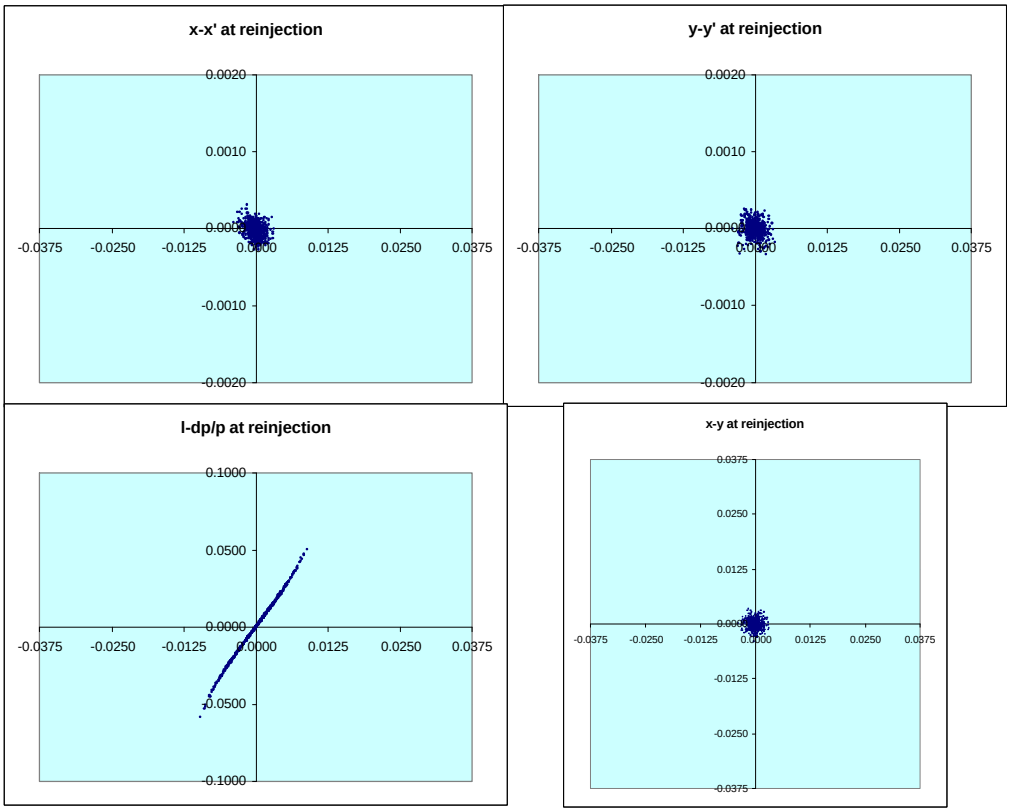

Figure 15a: Simulation of energy recovery: reinjection point

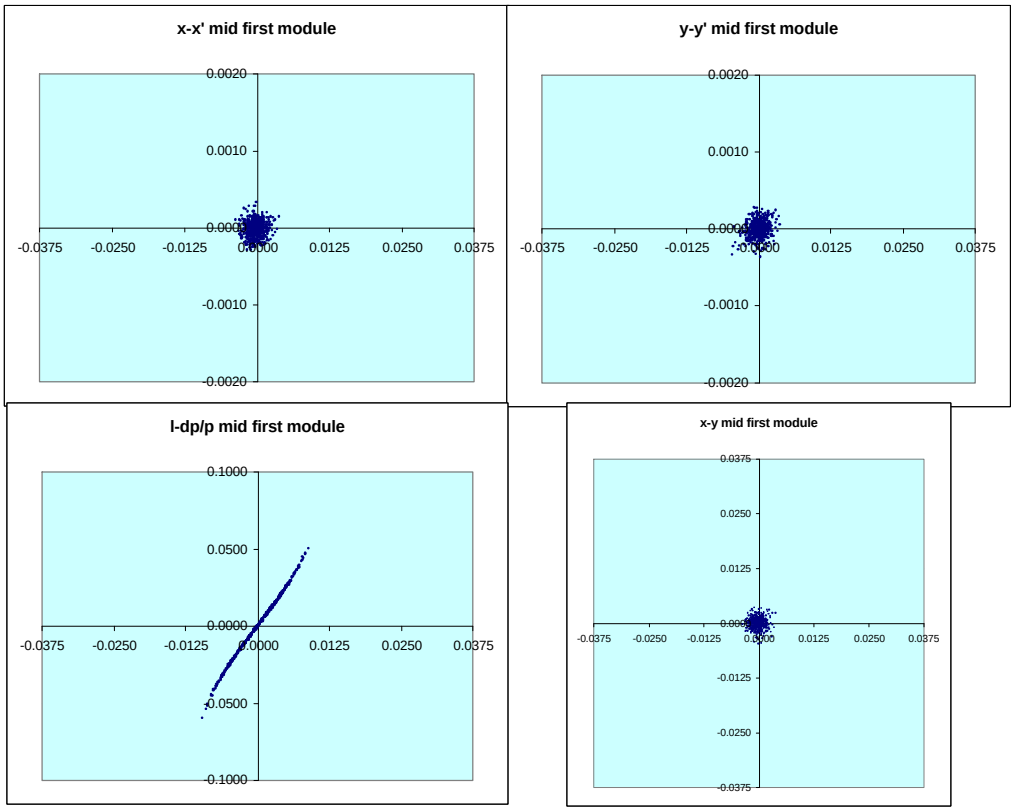

Figure 15b: Mid first module

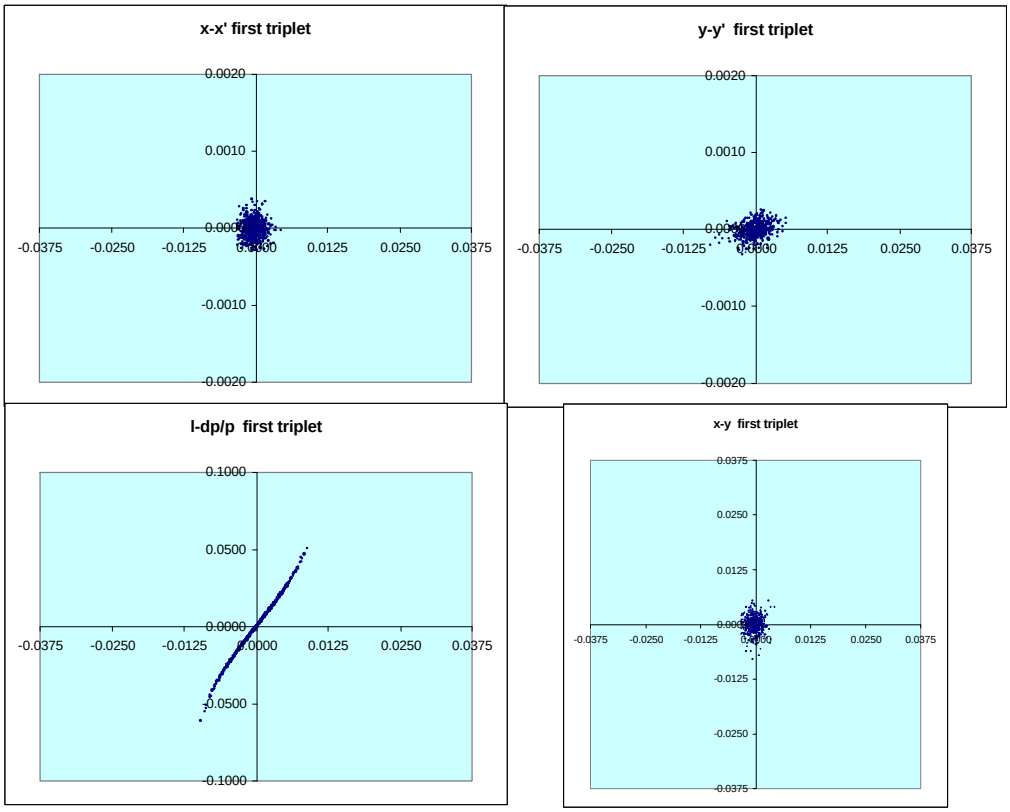

Figure 15c: Mid first triplet

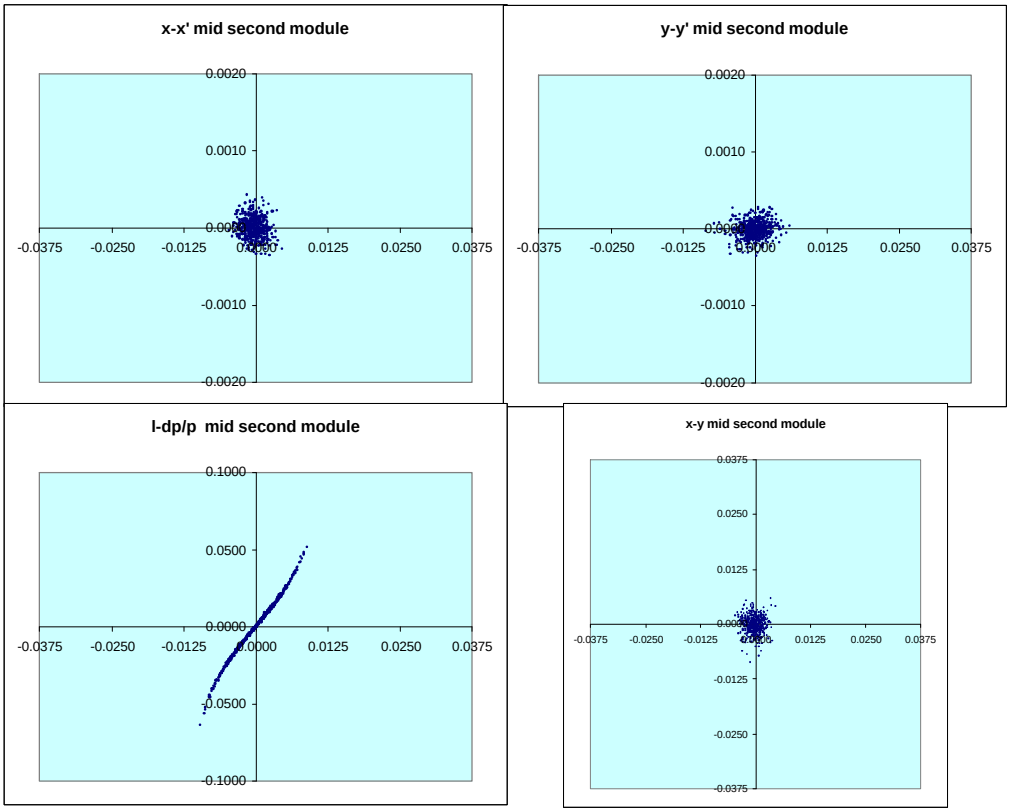

Figure 15d: Mid second module

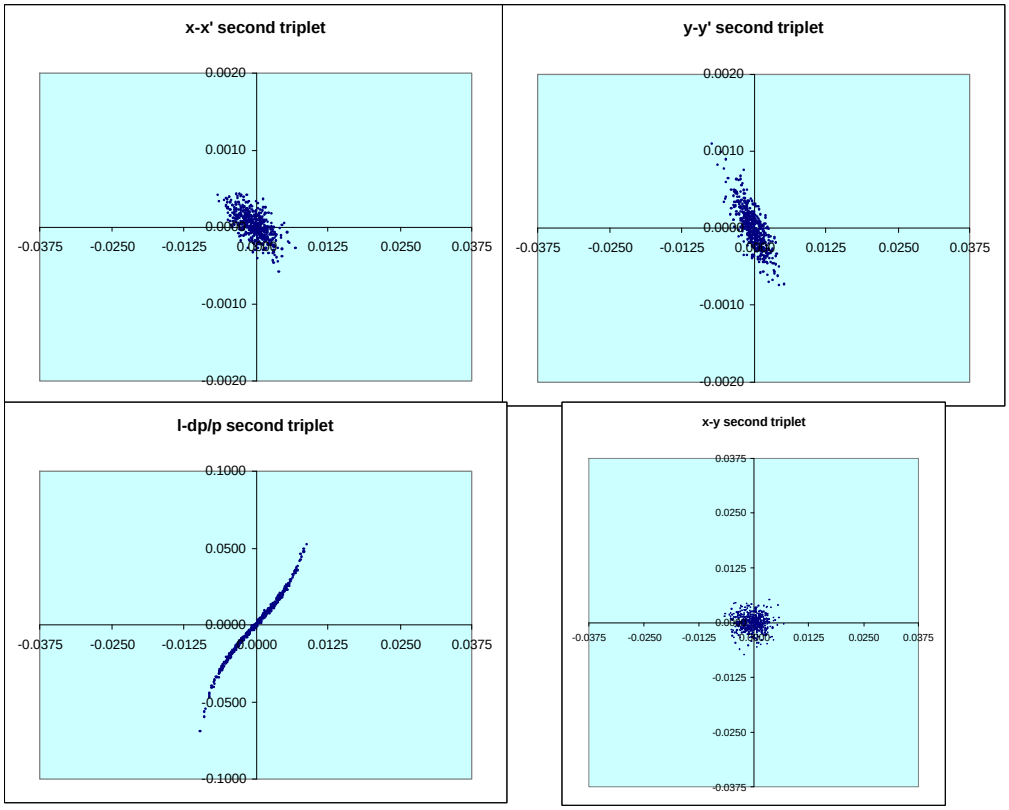

Figure 15e: Mid second triplet

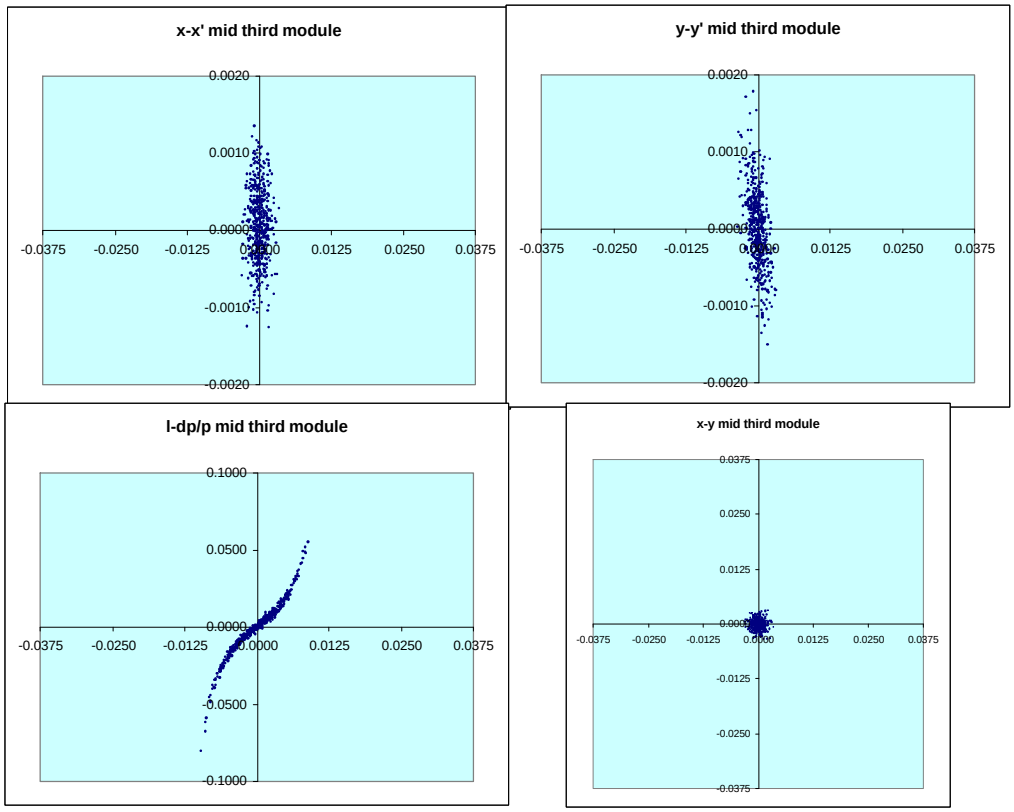

Figure 15f: Mid third module

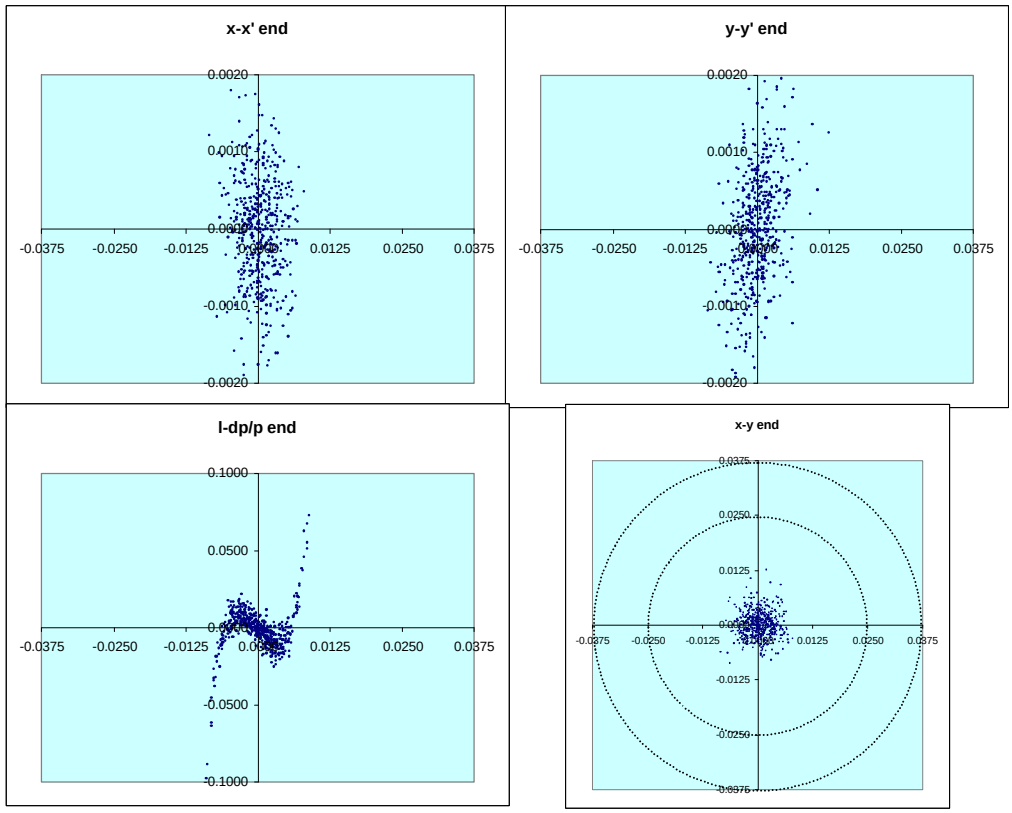

Figure 15g: Extraction point

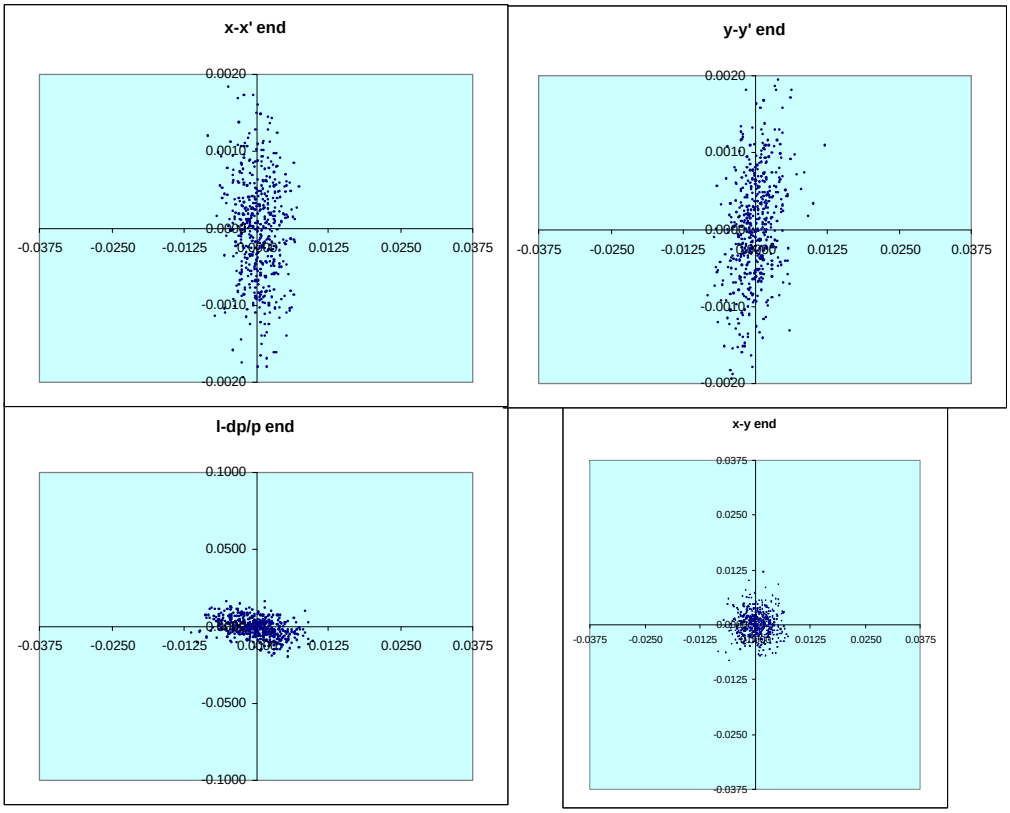

Figure 16: Extraction point – octupoles activated

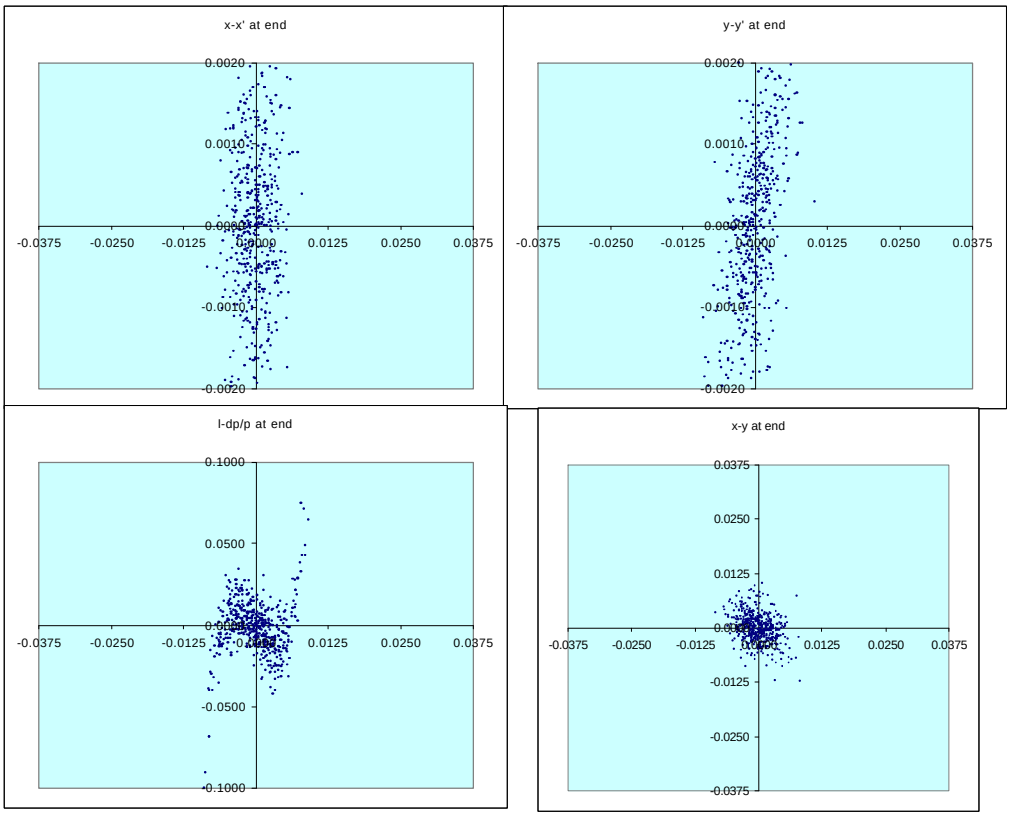

Figure 17: Extraction point – skew quad effects included

The above numerical analysis was performed using DIMAD. The astute reader may well enquire as to the validity of the results, given the low energies and large phase space volumes being simulated using a speed of light, second order code. To verify the results, a 4th order Runge-Kutta integrator was implemented as a VBA macro within MSExcel and an "exact" solution of the equations of motion performed for the transport system endloops. In this nonperturbative model, in particle positions are evaluated in the lab frame at finite velocity and the only major approximation was the use of hard-edged, ideal magnetic fields. Results for motion of a 20% momentum spread beam through an end loop are presented in Figure 18; comparison of the exact result with DIMAD is shown in Figure 19.

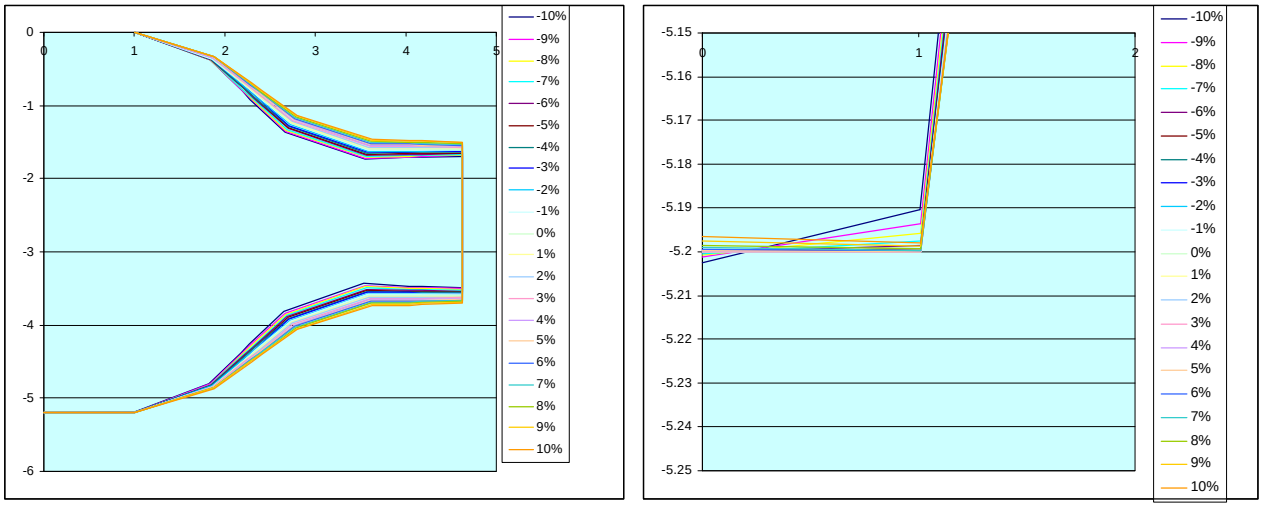

Figure 18: Results of "exact" solution for 20% momentum spread beam transported through recirculator endloop.

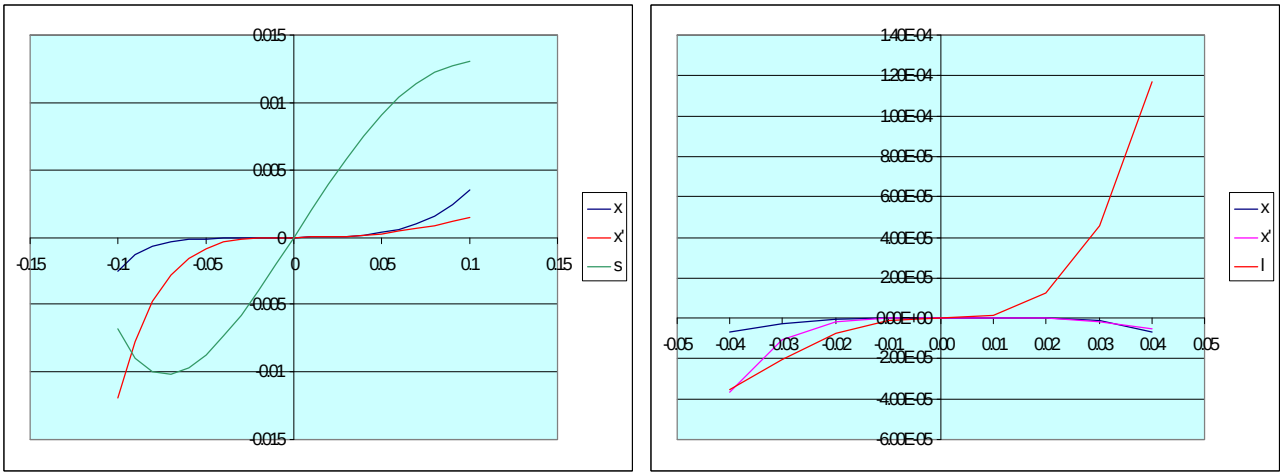

Figure 19: Comparison of exact (left) and DIMAD (as in Figure 14) results. Detailed examination demonstrates the agreement is at least third order (path length) or higher (transverse position and angle).

The agreement of DIMAD with exact solution of the equation of motion suggests the DIMAD "TURTLE-mode" tracking algorithm is adequate for simulation in the parameter space of this machine. Ongoing work will extend the integration over a larger portion of the energy-recovery transport and will evaluate focussing effects as well.

What's Missing from Revision 1.0

The following list summarizes known issues, omissions, interferences and discrepancies.

1) There is a need for further resolution of injection line geometry:
   a) we must check remnant dispersion due to use of rectangular dipoles and decide whether to tolerate it or correct it, and
   b) the injection/reinjection, extraction/recirculation chicane dipoles are optimized for a 10 MeV/c:160 MeV/c ratio – is this the "right" choice?
2) We must develop quantitative knowledge of maximum tolerable 1st and last module energy gains (establish limitations based on cavity focussing induced mismatch).
3) We must develop a model of 7-cell cavity dynamics.
4) The warm region slot lengths are presently configured to support only a center 7-cell modules; if the linac is to support further upgrades using outboard 7-cell modules, this should be reviewed (but keep "What's Missing" #2 in mind!).
5) This revision has optical cavity lengths and path length numerology for a 20th subharmonic drive laser frequency. Any design using drive laser frequencies other than the 20th subharmonic of the RF fundamental will require a rework.
6) This revision uses approximate (10% level) dipole field rolloff integrals ("fint") in beamline dipoles; as the dipole designs solidify the accuracy of this parameter should be improved [13].
7) We must resolve an interference between the big chicane and the upstream optical cavity end-can.
8) We presently plan to use IR Demo DW dipoles for the little chicanes; this design revision uses only approximate DW parameters in this location. Accuracy of these parameters should be improved.
9) The recirculation path length should be established; BBU thresholds may prefer a recirculation path length at the 10th odd subharmonic (630.5 λ_{RF}); multipass BPM operation may require something rather different.
10) The design has not been subjected to analysis of the effects of space charge, CSR, and BBU. A collective effects sanity check should be made before further major design revisions are performed.

Component Counts

Table 2 provides a summary component count and very sketchy description. The "Reference" column cites the information source for the component count or description.

Table 2: Revision 1.0 Component Counts

System/Component	Number	Description	Source
RF			
Buncher	1		IR Demo inheritance
Cryounit	1		IR Demo inheritance
Cryomodule	3	two 5-cell, one 7-cell	IR Demo inheritance, DIMAD, linac concept
Dipoles			
Small rectangular dipole	9	Injection/reinjection/extraction dipole	DIMAD, injection line concept
Small sector dipole	1	Injection line central dipole	Injection line concept
Sector reverse bends	8	4 normal entry 4 double focussing	DIMAD
π bends	2		DIMAD
Quadrupoles			
QJ	4	Injection match	IR Demo inheritance
Iron Quads	42	3” bore, 0.15 m long	DIMAD
Trim quads	8	Endloop trims	DIMAD
Sextupoles			
Endloop sextupoles	8	Endloop trims	DIMAD
Octupoles			
Endloop octupoles	2 (+2*)	Endloop trims	DIMAD
Correction Dipoles			
Pathlength correctors	4	Demo DG equivalents	concept
Horizontal/vertical steering	22/20***	Beamline steerers	4 x (phase advance)
Diagnostics			
BPMs	24***	20 standard (mix of 4 channel, SEE), 4 multipass	4 x (phase advance) + 2 at dump
BCM	5**	1 injector, 4 recirculator	concept
Happek Devices	2**		concept
OTR viewers, SLM monitors	39***	3 injector 4 linac (with holes) 4 in 1st telescope 3 in 1st endloop 6 in backleg 1 in big chicane 3 in upstream match 5 in wiggler 3 in downstream match 3 in 2nd endloop 4 in reinjection match	concept

* Second pair as contingency
** Approximate
*** Very, very approximate

Acknowledgments

I would like to thank other members of the FEL Upgrade design ensemble – Geoff Krafft, Ri Li, Lia Merminga, and Byung Yunn – and members of the Jefferson Lab FEL Department for useful input to, and discussions about, this design. I would also like to thank Butch Dillon-Townes, Jeff Karn, Jacki Smith and Robin Wines for repeated discussions, design information, and ongoing reality checks.

References

[1] See, for example, http://www.jlab.org/~douglas/FEL/FELmasterindex.html, a guide to which is available in D. Douglas, "A Guide to the FEL Driver E-Beam Optics Design Web Site", JLAB-TN-97-012", 10 March 1997. This is itself available at http://www.jlab.org/~douglas/FEL/technote/JLABTN07012.ps.

[2] D. Douglas, "WBS 3.0: Beam Physics Requirements for the IR Upgrade Driver Accelerator", JLAB-TN-00-012, 31 May 2000.

[3] In the IR Demo, the error budget was specified to insure that performance was sufficient, though perhaps better than necessary, to meet the machine performance goals. Thus for example, individual error sources were in general constrained to limit degradation of any particular beam performance parameter (for example, beam envelopes) to the ~10% level over the full machine. We thereby limited beam quality degradation at the wiggler to ~10% and through the machine to a factor of ~2. This level of control was in general achievable through the use of CEBAF standard tolerances on power supplies and trim magnets; main dipole field quality specifications required the use of cutting (though not bleeding) edge techniques. Further information is provided at the site in Reference 1; of particular use will be the following technical notes: CEBAF-TN-95-071, CEBAF-TN-96-018, CEBAF-TN-96-026, CEBAF-TN-96-035, CEBAF-TN-055, CEBAF-TN-96-059, JLAB-TN-96-066, JLAB-TN-97-015, JLAB-TN-97-034, JLAB-TN-97-035, JLAB-TN-98-004, and JLAB-TN-98-042, all of which are available from http://www.jlab.org/~douglas/FEL/technote/technoteindex.html. We expect to use the same error budget and specifications in this machine.

[4] D. Douglas, "Aperture Considerations for the FEL Upgrade", JLAB-TN-99-043, 15 December 1999.

[5] B. Yunn, private communication.

[6] D. Douglas, "IR/UV FEL Upgrade Project Accelerator Physics Plan", JLAB-TN-99-041, 2 December 1999; D. Douglas, "WBS 3.0: Beam Physics Requirements for the IR Upgrade Driver Accelerator", *op. cit.*

[7] D. Douglas, “A Driver Accelerator for an FEL Upgrade”, JLAB-TN-99-019, 21 July 1999.

[8] J. Karn, private communication.

[9] D. Douglas, “Modeling of Longitudinal Phase Space Dynamics in Energy-Recovering FEL Drivers”, JLAB-TN-99-002, 14 January 1999.

[10] It is likely, for example, that a nontrivial portion of the bunch length at the IR Demo wiggler is due to RF waveform curvature in the acceleration. See, for example, Figures 6 and 7 of the previous reference.

[11] D. Douglas, “Modeling of Longitudinal Phase Space Dynamics in Energy-Recovering FEL Drivers”, *op. cit.*

[12] We intend to perform a study of the type documented in D. Douglas, “Effect and Compensation of HOM-Generated Skew Quadrupole Fields in the CEBAF Linacs”, CEBAF-TN-95-037, 13 June 1995.

[13] Jeff Karn has provided more precise values; given the preliminary state of the design, I used only the “order of magnitude” of his information. Better resolution will be used in the next design revision. I promise. Trust me. Really. It’ll be okay. Don’t worry.